JACS
JOURNAL OF THE AMERICAN CHEMICAL SOCIETY

Subscriber access provided by BIU Pharmacie | Faculté de Pharmacie, Université Paris V

Article

Extraordinary Acceleration of Cogwheel Helical Self-Organization of Dendronized Perylene Bisimides by the Dendron Sequence Encoding their Tertiary Structure

Li Wang, Benjamin E. Partridge, Ning Huang, James T Olsen, Dipankar Sahoo, Xiangbing Zeng, Goran Ungar, Robert Graf, Hans W. Spiess, and Virgil Percec

J. Am. Chem. Soc., **Just Accepted Manuscript** • Publication Date (Web): 28 Apr 2020

Downloaded from pubs.acs.org on April 28, 2020

Just Accepted

"Just Accepted" manuscripts have been peer-reviewed and accepted for publication. They are posted online prior to technical editing, formatting for publication and author proofing. The American Chemical Society provides "Just Accepted" as a service to the research community to expedite the dissemination of scientific material as soon as possible after acceptance. "Just Accepted" manuscripts appear in full in PDF format accompanied by an HTML abstract. "Just Accepted" manuscripts have been fully peer reviewed, but should not be considered the official version of record. They are citable by the Digital Object Identifier (DOI®). "Just Accepted" is an optional service offered to authors. Therefore, the "Just Accepted" Web site may not include all articles that will be published in the journal. After a manuscript is technically edited and formatted, it will be removed from the "Just Accepted" Web site and published as an ASAP article. Note that technical editing may introduce minor changes to the manuscript text and/or graphics which could affect content, and all legal disclaimers and ethical guidelines that apply to the journal pertain. ACS cannot be held responsible for errors or consequences arising from the use of information contained in these "Just Accepted" manuscripts.

is published by the American Chemical Society. 1155 Sixteenth Street N.W., Washington, DC 20036
Published by American Chemical Society. Copyright © American Chemical Society. However, no copyright claim is made to original U.S. Government works, or works produced by employees of any Commonwealth realm Crown government in the course of their duties.

Extraordinary Acceleration of Cogwheel Helical Self-Organization of Dendronized Perylene Bisimides by the Dendron Sequence Encoding their Tertiary Structure

Li Wang,[†,○] Benjamin E. Partridge,[†,□] Ning Huang,[†] James T. Olsen,[†] Dipankar Sahoo,[†] Xiangbing Zeng,[§] Goran Ungar,[§,#] Robert Graf,[◊] Hans W. Spiess[◊] and Virgil Percec[†,*]

[†] Roy & Diana Vagelos Laboratories, Department of Chemistry, University of Pennsylvania, Philadelphia, Pennsylvania 19104-6323, United States

[○] College of Materials Science and Engineering, Beijing University of Chemical Technology, Beijing 100029, China

[§] Department of Materials Science and Engineering, University of Sheffield, Sheffield, S1 3JD, United Kingdom

[#] State Key Laboratory for Mechanical Behavior of Materials, Xi'an University, Xi'an 710049, China

[◊] Max-Planck Institute for Polymer Research, 55128 Mainz, Germany

*E-mail: percec@sas.upenn.edu

ABSTRACT: The cogwheel model of hierarchical self-organization provides a route to highly ordered crystalline helical columnar hexagonal arrays of perylene bisimides (PBIs) conjugated to (3,4,5)-dimethyloctyl (racemic dm8*, **r**) minidendrons. Cogwheel PBIs assemble with identical structural order irrespective of molecular chirality to generate helical columns jacketed with an alkyl coat with length equal to half the helical pitch, exhibiting helical deracemization in crystal state. These assemblies were accessible only *via* annealing or cooling and reheating at 1 °C/min. Recently it was discovered that hybrid **rr8** sequence-defined dendrons with **r** and linear *n*-octyl (**8**) chains enabled the formation of the cogwheel phase at 10 °C/min upon heating but not cooling. Here we report four libraries of hybrid PBIs with sequence-defined dendrons containing **r** and *n*-alkyl (C_nH_{2n+1}) chains with n = 6, 7, 9, and 10. Structural analysis of these libraries by fiber X-ray diffraction and differential scanning calorimetry reveals that **9r9** sequence enables an extraordinary acceleration of cogwheel assembly at rates of up to 50 °C/min on heating and cooling, providing, to the best of our knowledge, the fastest crystallizing supramolecular or covalent macromolecule known. Solid state NMR studies help to elucidate this unexpected and unprecedented extraordinary acceleration of hierarchical self-organization, which arises from a combination of crystal packing of the ideal tertiary structure and alkyl chain dynamics. This general model raises questions about the use of achiral motifs to achieve high structural order in chiral systems and the need for disorder to create order in complex biological and bioinspired synthetic systems.

INTRODUCTION

Function in natural systems arises from the hierarchical transfer of structural information encoded in a primary structure, such as DNA or an amino acid sequence, and expressed by a tertiary structure, such as the folded state of a protein.[1] These structures are often helical[2] and are invariably homochiral, the origin of which remains one of the greatest unsolved fundamental questions within the natural sciences.[3] The emergence of homochiral life necessitates a means to resolve chirality within racemic mixtures, by enriching a statistical chiral imbalance[4] or by separating racemates into enantiopure domains.[5] This separation – known as deracemization – was demonstrated for the first time in the solution state by Pasteur in the 1840s.[6]

Supramolecular polymers[7] provide a tunable platform for exploring helical assembly,[8] responsive materials,[9] and the role of chirality in generating order.[10] Deracemization in the crystal state of supramolecular systems was first observed recently for racemic mixtures of hat-shaped dendronized molecules,[11] and was driven by the demand of the hexagonal unit cell of the columnar crystal that all columns be identical, exhibiting the same helical sense, within each crystal domain. The mechanism of deracemization, which depended on weak interactions between individual molecules, could only be understood using solid state NMR.[12] Supramolecular deracemization does not occur in systems with strong intermolecular interactions, such as chiral dendritic dipeptides,[13] which instead give lower order assemblies when not enantiopure.[14] Indeed, incomplete deracemization of mixtures of hat-shaped molecules containing inseparable, diastereomeric combinations of stereocenters gave reduced order in the crystal state. This observation is analogous to the amorphous nature of atactic poly(propylene) compared to the crystallinity of its isotactic counterpart.[15]

Subsequently a perylene bisimide (PBI)[16] with two chiral minidendrons[17] that assembles into 3D helical columnar hexagonal ($\mathbf{\Phi_h}$) arrays with identical single crystal-like order irrespective of molecular chirality

was discovered (Figure 1a).[18] The $\mathbf{\Phi_h}$ array exhibited helical deracemization, whereby even statistical mixtures of all possible diastereomers generated crystalline domains with a single helical sense.

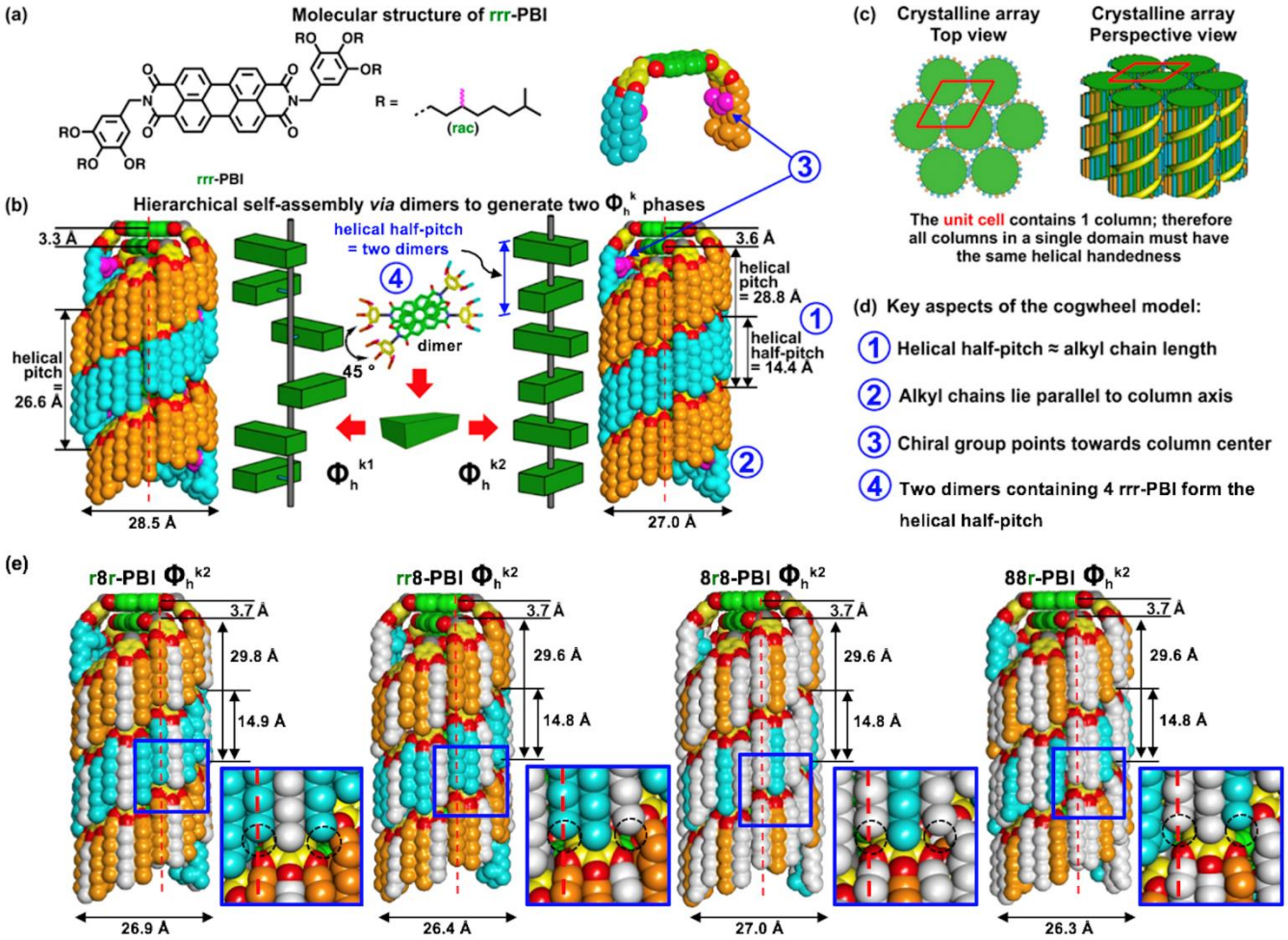

Figure 1. The cogwheel model of self-organization. (a) Molecular structure of **rrr-PBI** where **r** stands for racemic dm8*. Chiral methyl group is indicated in pink. (b) The two crystalline columnar hexagonal ($\mathbf{\Phi_h^k}$) phases are generated *via* hierarchical self-organization of PBI dimers rotated around the column axis being offset from the column axis in $\mathbf{\Phi_h^{k1}}$ and centered on the column axis in $\mathbf{\Phi_h^{k2}}$. Due to its columnar shape and the absence of alkyl groups perpendicular or tilted to the long axes of the column, intercolumnar interdigitation of alkyl chains is absent and therefore, we denote $\mathbf{\Phi_h^{k2}}$ as the "cogwheel" assembly. (c) Formation of a $\mathbf{\Phi_h^k}$ array with only one helical column in the unit cell drives helical deracemization between columns. (d) Key aspects of the cogwheel model. (e) The supramolecular columns assembled from **r8r-**, **rr8-**, **8r8-**, and **88r-PBI**[19], where **8** represents the *n*-octyl group, and insets illustrating the incomplete space filling by the alkyl ends from the 3- and 5- positions of the dendron. Dashed circles in insets indicate empty space on the column periphery. Panels (a)–(d) are adapted from ref. 19.

This chirality-invariant structural order was rationalized using a model in which alkyl chains on the periphery of the supramolecular column act like the "teeth" of a cogwheel, covering the exterior of a

column assembled from molecular dimers (Figure 1b). X-ray diffraction (XRD) and variable rate differential scanning calorimetry (DSC) experiments confirmed that the cogwheel phase (denoted $\mathbf{\Phi_h^{k2}}$), which was discovered by chance during XRD annealing studies, is formed only by annealing at 100 °C or upon slow cooling and reheating at 1 °C/min.

This *cogwheel model* had not been observed in assemblies of PBIs with exclusively linear *n*-alkyl chains that interdigitate,[20] likely because the key attributes of the *cogwheel model* (Figure 1d) not only demand peripheral alkyl chains which lie parallel to the column axis and are of approximately equal length to the half-pitch of the helical column, but also depend on the chiral methyl group of the dimethyloctyl (dm8*) chain to efficiently fill space within the center of the column and adopt an appropriate secondary structure that may disfavor intercolumnar interdigitation[21] of chains (Figure 1a). Therefore, PBIs with sequence-defined hybrid dendrons containing mixtures of linear *n*-octyl and dm8* chains were investigated, leading both to the discovery that linear alkyls can be tolerated together with dimethyloctyl by the cogwheel assembly and, in addition, to a hybrid sequence of dm8*/linear chains that forms the cogwheel $\mathbf{\Phi_h^{k2}}$ phase under relatively fast heating and cooling at 10 °C/min with the phase transition being observed only on heating (Figure 1e).[19] However, the role of the linear alkyl chain in accelerating the formation of the cogwheel $\mathbf{\Phi_h^{k2}}$ phase remained unclear and raised the question: how do linear *n*-alkyl chains affect assembly *via* the cogwheel model?

To answer this question, this study reports the investigation of four libraries of hybrid PBIs with sequence-defined mixtures of racemic dm8*, **r**, chains and linear *n*-alkyl (C_nH_{2n+1}) chains with n = 6, 7, 9, and 10 carbons in the alkyl group. Structural and retrostructural analysis of these libraries by XRD and DSC reveals a dendron sequence that enables an extraordinary acceleration of the formation of the cogwheel $\mathbf{\Phi_h^{k2}}$ phase at rates of up to 50 °C/min. *This is the highest rate that any current instrumentation including DSC and XRD can be used for quantitative, temperature dependent structural analysis in conventional*

research laboratories. Together with solid state NMR and previous work with **r**/*n*-octyl dendrons,[19] this extraordinary acceleration of the rate of $\mathbf{\Phi_h^{k2}}$ formation relies on a complex interplay of crystal packing and chain dynamics. These findings raise questions about the role of non-chiral building blocks in achieving a high degree of structural order in chiral systems, support the power of constitutional isomerism to dictate self-assembly.[19,22] and provide insights into the design of highly ordered assemblies with extraordinary acceleration of their formation and bulk helical deracemization.

Synthesis of Libraries of PBIs Containing Sequence-Defined Hybrid Dendrons. Defining the sequence[23] of biological and bioinspired molecules is a powerful means to control supramolecular assembly[24] and elucidate fundamental biological concepts such as protein-carbohydrate binding.[25] Here, sixteen sequence-defined hybrid dendronized PBIs were synthesized using an iterative methodology elaborated in a previous communication (Scheme 1).[19]

The nomenclature for these PBIs is dictated by the alkylation pattern on the (3,4,5)-minidendron, using **r** to denote the **r** chain and ***n*** to denote a linear *n*-alkyl, C_nH_{2n+1}, where n = 6, 7, 9, or 10. This functionalization pattern, or sequence of alkyl chains on the dendron periphery, is uniquely defined during synthesis. Sequence-defined dendrons **5** were prepared either from symmetrically-protected methyl gallate derivative **2** (for **r*n*r-** and ***nrn*-PBI**) or its asymmetrically-protected analog **6** (for **rr*n*-** and ***nn*r-PBI**). These four sequences should not be interconverted just like in the case of proteins and are independent of each other irrespective of dendron rotation. Alkylation with an initial alkyl chain, followed by deprotection and a second alkylation, provided dendrons **5**. Functional group manipulation of the benzyl esters **5** to benzyl amines **12**, and subsequent imidation of perylene tetracarboxylic dianhydride (PTCDA) per procedures elaborated in our laboratory,[20a] gave PBIs with sequence-defined dendrons (Figures S1–S48).

Scheme 1. Synthesis of PBIs with Sequence-Defined Linear-Racemic Hybrid Minidendrons[a]

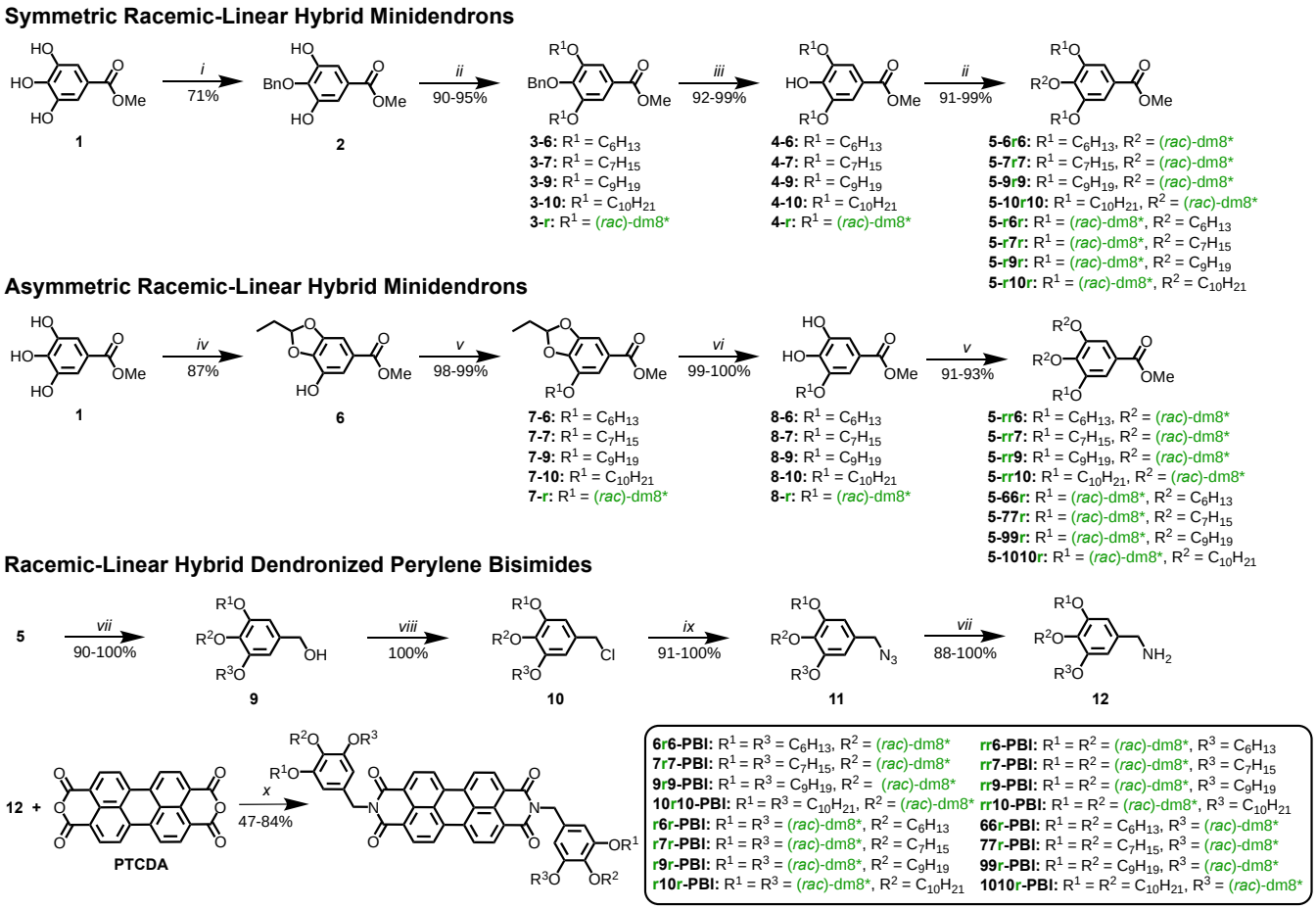

[a]Reagents and conditions: (*i*) BnCl, $KHCO_3$, DMF, 60 °C, 24 h; (*ii*) RBr, K_2CO_3, DMF, 120 °C, 3.5–12 h; (*iii*) H_2, Pd/C, CH_2Cl_2/MeOH, 23 °C, 24 h; (*iv*) triethyl orthoformate, Amberlyst-15(H), toluene, reflux, 6 h; (*v*) RBr, K_2CO_3, DMF, 65–70 °C, 4 h; (*vi*) HCl, methanol, 60 °C, 7 h; (*vii*) $LiAlH_4$, THF, 23 °C, 1 h; (*viii*) $SOCl_2$, cat. DMF, 23 °C, CH_2Cl_2, 0.5 h; (*ix*) NaN_3, DMF, 23 °C, 9 h; (*x*) PTCDA, $Zn(OAc)_2$•$2H_2O$, imidazole, 180 °C, 6 h.

The Discovery of the Extraordinary Acceleration of the Cogwheel Self-Organization. The thermal analysis of the sixteen PBIs with hybrid dendrons (n = 6, 7, 9, 10), as well as fully racemic **rrr-PBI**, fully linear ***nnn*-PBI** (n = 6–10),[20c] and hybrid *rac*-dm8*/*n*-octyl dendrons,[19] was determined by DSC (Figures 2, 3, and S49–S57 and Supporting Table ST1).

Phases were assigned by XRD and will be discussed later. Whereas the cogwheel $\mathbf{\Phi_h^{k2}}$ phase was observed for all four hybrid PBIs with *n*-octyl chains upon both heating and cooling (Figures S51 and S56), changing the length of the alkyl chain to n = 6, 7, or 10 eliminates the $\mathbf{\Phi_h^{k2}}$ phase from all hybrid dendron sequences except **rr*n*-PBI**, for which $\mathbf{\Phi_h^{k2}}$ is observed only upon heating (Figures S49, S50, and S53).

Changing the alkyl chain to *n*-nonyl also generates the $\mathbf{\Phi_h^{k2}}$ cogwheel phase in **rr9-PBI** and in **9r9-PBI** (Figures 2 and S52). This observation suggests that (1) there is something inherent in the **rr*n***-sequence that tolerates different alkyl chain lengths, and (2) alkyl chains that are 8 or 9 carbons in linear length (i.e. dimethyl*octyl*, *n*-octyl, and *n*-nonyl) are best tolerated by the cogwheel model in other dendron sequences. The DSC traces of **rr*n*-PBI** (*n* = 6-9; Figures S49-S52) all exhibit an endothermic peak at about 140 °C upon heating, assigned to the first order transition from the cogwheel $\mathbf{\Phi_h^{k2}}$ phase to a lower order columnar hexagonal phase, $\mathbf{\Phi_h^{k1}}$ (Figure 1b, left). A corresponding exothermic crystallization peak upon cooling is not observed, suggesting that crystallization into the $\mathbf{\Phi_h^{k2}}$ phase is a continuous, very slow process occurring under kinetic control. By contrast, the DSC trace of **9r9-PBI** upon cooling (Figures 2 and S52) shows a distinct crystallization exotherm at 107 °C, suggesting that the transition from low order $\mathbf{\Phi_h^{k1}}$ to high order cogwheel $\mathbf{\Phi_h^{k2}}$ is well-defined, even upon fast cooling (10 °C/min).

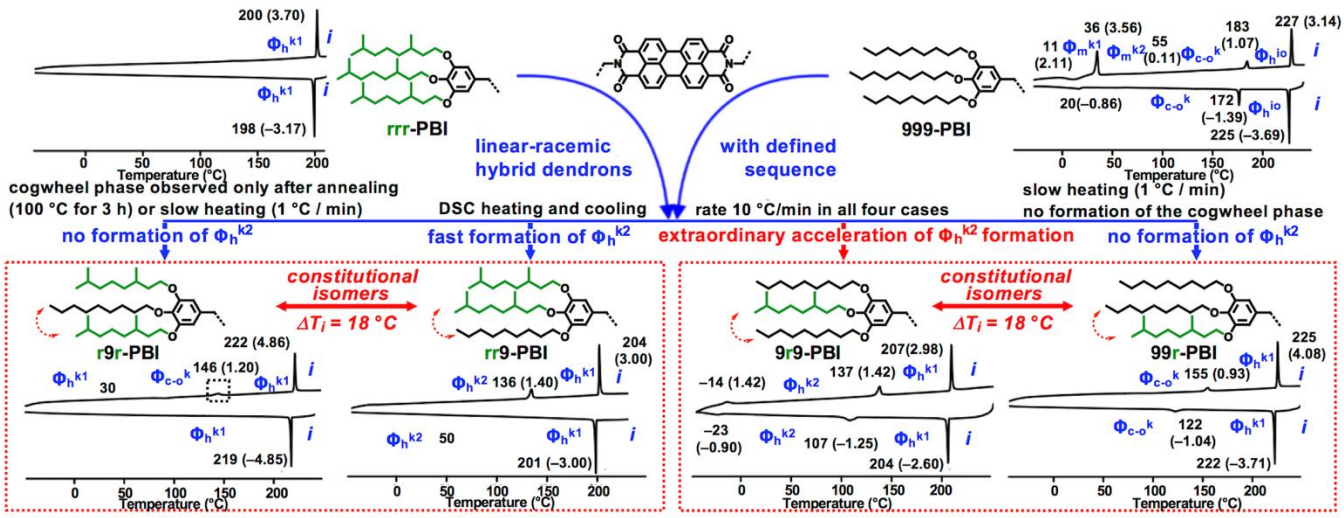

Figure 2. DSC traces of PBIs with sequence-defined hybrid **r**/*n*-nonyl dendrons recorded upon second heating and first cooling at 10 °C/min. Phases determined by fiber XRD, transition temperatures (in °C), and associated enthalpy changes (in parentheses, in kcal/mol) are indicated. Phase notation: $\mathbf{\Phi_h^{k1}}$-columnar hexagonal crystal with offset dimers; $\mathbf{\Phi_h^{k2}}$-columnar hexagonal crystal with cogwheel assembly; $\mathbf{\Phi_{c\text{–}o}^{k}}$-columnar centered orthorhombic crystal; $\mathbf{\Phi_m^{k}}$ - columnar monoclinic crystal, ***i***-isotropic liquid.

To probe the kinetics of the $\mathbf{\Phi_h^{k1}}$–$\mathbf{\Phi_h^{k2}}$ transition in **9r9-PBI** based assemblies, DSC traces were measured at rates from 10 to 50 °C/min (Figure 3). Unexpectedly, a discrete exothermic crystallization peak is

observed at the transition between $\mathbf{\Phi_h^{k1}}$ and $\mathbf{\Phi_h^{k2}}$ upon cooling at all rates. The enthalpy of the transition (1.04 kcal/mol) does not vary for cooling rates from 20 to 50 °C/min, although the transition temperature decreases from 103 °C at 20 °C/min to 96 °C/min at 50 °C/min. It should be noted that 11 °C of extra supercooling necessary to form the $\mathbf{\Phi_h^{k2}}$ phase at 50 *vs* 10 °C/min (compare T_{onset} of 96 and 107 °C) represents only a 15-second delay in the onset of the phase transition at 50 °C/min. These data suggest that the $\mathbf{\Phi_h^{k1}}$-$\mathbf{\Phi_h^{k2}}$ transition for **9r9-PBI** assemblies was extraordinarily accelerated and is much faster than has been observed for any other cogwheel assembly including homochiral.

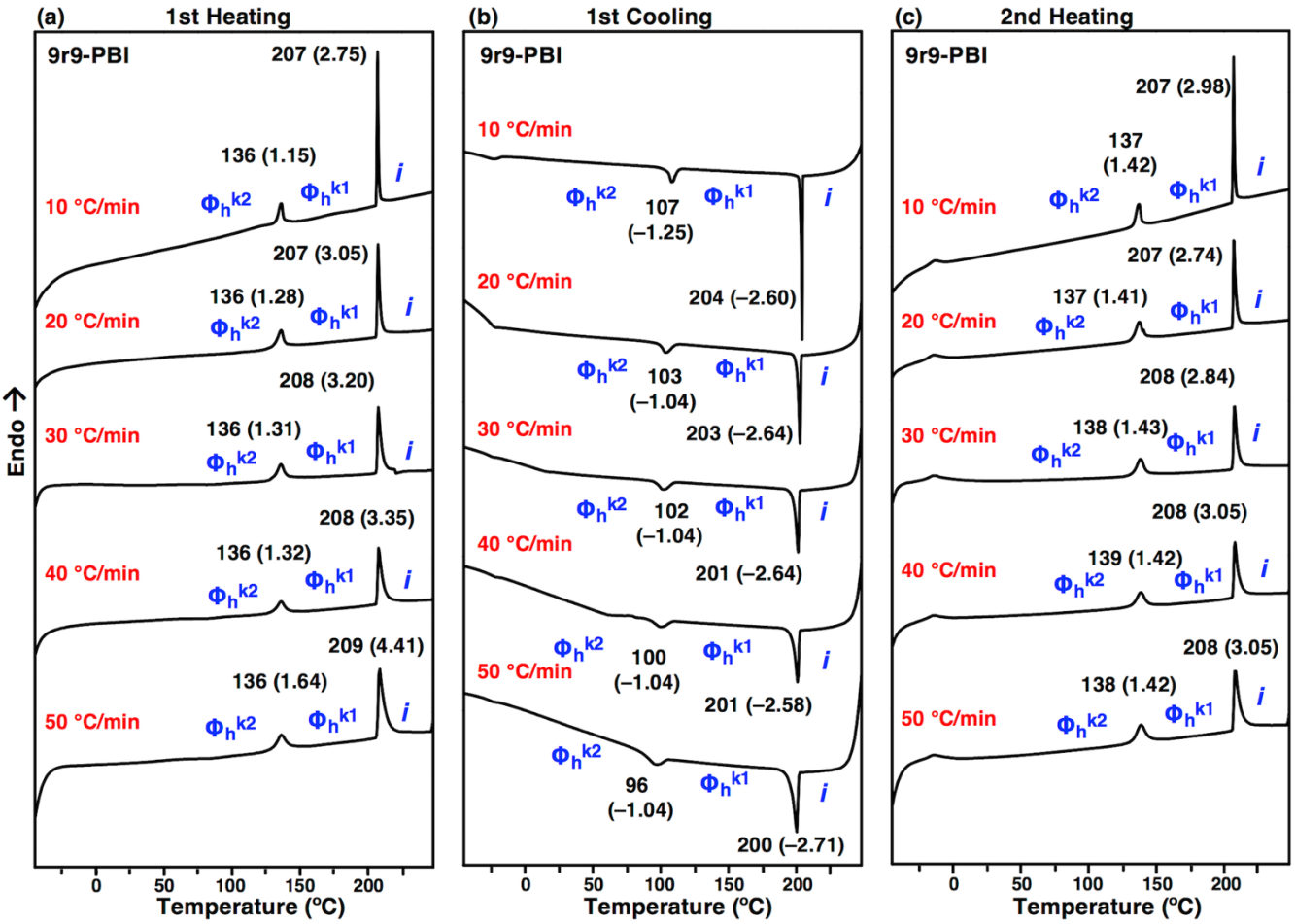

Figure 3. DSC traces of **9r9-PBI** assemblies measured upon heating and cooling at 10 to 50 °C/min during (a) 1st heating, (b) 1st cooling, and (c) 2nd heating. Phases determined by fiber XRD, transition temperatures (in °C), and associated enthalpy changes (in parentheses, in kcal/mol) are indicated. Phase notation: $\mathbf{\Phi_h^{k1}}$ – columnar hexagonal crystal with offset dimers; $\mathbf{\Phi_h^{k2}}$ – columnar hexagonal crystal with cogwheel assembly; $\mathbf{\Phi_{c-o}^{k}}$ – columnar centered orthorhombic crystal; $\mathbf{\Phi_m^{k}}$ – columnar monoclinic crystal, ***i*** – isotropic liquid.

Structural and Retrostructural Analysis by XRD Confirms High-Order Helical Cogwheel Assembly Irrespective of Rate. The phases annotated on all DSC traces were determined by XRD of oriented fibers.[~~25~~26] Fiber XRD diffractograms for PBIs with hybrid **r**/*n*-nonyl dendrons are shown in Figure 4. In each case, a higher order phase is observed at low temperature (columnar centered orthorhombic, $\mathbf{\Phi_{c-o}^{k}}$, for **r9r-** and **99r-PBI**; cogwheel $\mathbf{\Phi_{h}^{k2}}$ for **rr9-** and **9r9-PBI**) and the lower order $\mathbf{\Phi_{h}^{k1}}$ phase is observed at higher temperature (Supporting Tables ST2–ST4). The XRD data for **rr9-** and **9r9-PBI** are both consistent with the cogwheel $\mathbf{\Phi_{h}^{k2}}$ and lower order $\mathbf{\Phi_{h}^{k1}}$ phases observed previously.[18,19]

Reconstruction of the XRD by the molecular models depicted in Figure 5 support the description of the higher order phases as cogwheel phases (Figure 4, grayscale images on right). The $\mathbf{\Phi_{c-o}^{k}}$ phase observed for **r9r-** and **99r-PBI** is a pseudohexagonal phase that represents a distortion of a hexagonal array along the *a*- or *b*-direction of the unit cell. The ratio of *b*/*a* for a $\mathbf{\Phi_{c-o}^{k}}$ unit cell that is equivalent to a perfect $\mathbf{\Phi_{h}^{k}}$ cell would be 1.73 (= √3). For **r9r-** and **99r-PBI** this ratio is 1.60 and 1.61, respectively, suggesting a consistent deviation from a hexagonal array as dictated by the cogwheel model. However, the high number of sharp, bright off-axis features supports a high degree of order in these $\mathbf{\Phi_{c-o}^{k}}$ arrays rivalling that of the cogwheel phase.

To correlate the DSC traces from Figure 3 with the structure of **9r9-PBI**, diffractograms of the cogwheel $\mathbf{\Phi_{h}^{k2}}$ phase were measured at 100 °C upon first heating and cooling at rates of 10 to 40 °C/min (Figure S58). The XRD data shown in Figure 4 were recorded at 100 °C, heated at 10 °C/min and with 2 × 2.5 min recording time. The time it takes to record XRD patterns with reasonable signal/noise ratio means that we were not able to monitor the formation of the $\mathbf{\Phi_{h}^{k2}}$ phase in real-time by XRD at high heating/cooling rates. However, pleasingly, near-identical XRD patterns are observed at 100 °C, irrespective of heating and cooling rate (Figure S58). This demonstrates the extraordinary acceleration of the formation of the cogwheel $\mathbf{\Phi_{h}^{k2}}$ of **9r9-PBI**.

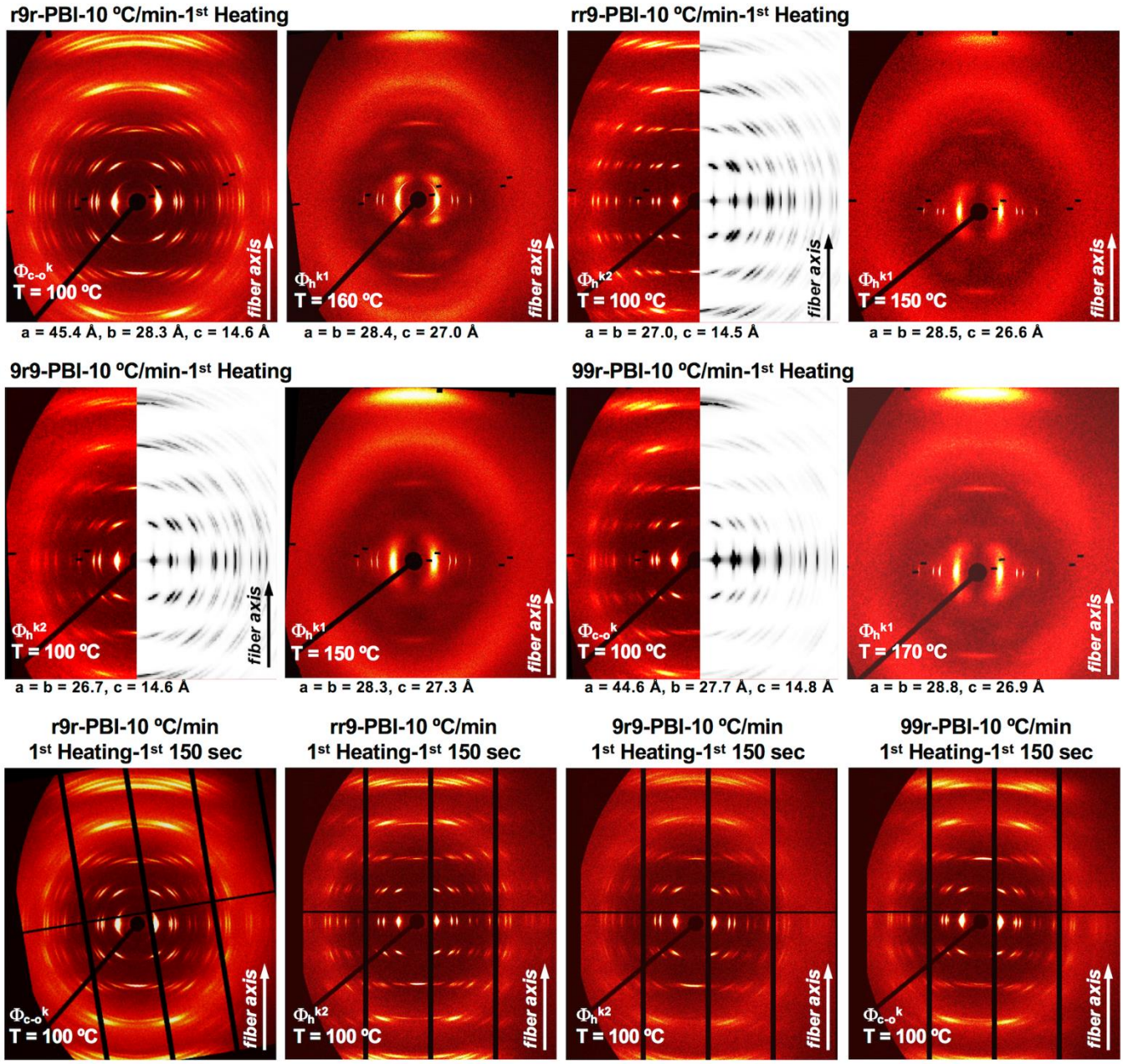

Figure 4. Fiber XRD of **9r9-PBI** assemblies measured upon heating and cooling at 10 °C/min (red scale, left) and XRD simulated from the models in Figure 5 (gray scale, right). Phases, lattice parameters, and temperatures (in °C) are indicated. The time employed to record each XRD is 5 min. The 5 min scan consists of two 2.5 min XRD scans. In a single 2.5 min scan, gaps between eight individual panels in the detector (Pilatus 1M, Dectris) are recorded as black stripes with no data. The detector is moved for a subsequent 2.5 min scan, which collects data in the previously unrecorded areas. The combination of the two 2.5 min scans provides a 5 min scan in which the black stripes are mostly eliminated.

To illustrate the practical implication of this rate acceleration, we consider how long it would take to obtain a macroscopic fiber of the cogwheel $\mathbf{\Phi_h^{k2}}$ phase of **rrr-PBI**,[18] **rr8-PBI**,[19] and **9r9-PBI** at 25 °C.

Starting with a freshly extruded macroscopic fiber at 25 °C, **rrr-** and **rr8-PBI** require heating to 100 °C (i.e. 7.5 min at 10 °C/min), followed by annealing for 3 hours and 30 min, respectively. After cooling to 25 °C at 10 °C/min (7.5 min), fibers of $\mathbf{\Phi_h^{k2}}$ would have been prepared in ~3 hours and 15 min for **rrr-PBI** and ~45 min for **rr8-PBI**. In contrast, Figure 4 shows that **9r9-PBI** transforms into $\mathbf{\Phi_h^{k2}}$ within 150 s at 100 °C. Therefore, including heating and cooling at 50 °C/min (90 s between 25 °C and 100 °C) the total time is only 330 seconds, i.e. 5.5 min. Reducing the processing time from over 3 hours for **rrr-PBI**[18] to ~5 min for **9r9-PBI** represents a substantial time saving that demonstrates how molecular design can affect both fundamentally- as well as industrially-relevant time-saving material parameters.

Structural Basis for Accelerated Cogwheel Formation in Assemblies of 9r9-PBI. To gain insight about the structural basis for the rapid formation of the cogwheel $\mathbf{\Phi_h^{k2}}$ by **9r9-PBI**, molecular models of supramolecular assemblies were generated using an iterative methodology described previously.[26,27] Diffraction features and lattice parameters were determined from fiber XRD data using Datasqueeze[28] and analyzed using helical diffraction theory.[2a,26,29] An initial molecular model consistent both with XRD data and with the experimental density of the macroscopic fiber was constructed using Accelrys Materials Studio software (version 5.0).[17c,26] Geometry optimization was performed using the VAMP module. The fiber XRD pattern expected from this model was simulated using Accelrys Cerius2 run on a Silicon Graphics (SGI) Tezro workstation.[11,17c] The simulated and experimental XRD patterns were compared,[11] the molecular model refined, and the XRD pattern simulated again. This iterative process continued until either the level of agreement between simulated and experimental XRD patterns was agreeable and no substantial improvement was observed upon further iteration.

Models of $\mathbf{\Phi_h^{k2}}$ phases observed in **rr*n*-PBI** (*n* = 6–10) and **9r9-PBI** reveal subtle differences in the alkyl chain periphery of their supramolecular columns (Figure 5). The column diameters of **rr*n*-PBI** generally increase with increasing linear alkyl chain length, from 25.4 Å (**rr6-PBI**) to 28.5 Å (**rr10-PBI**). The

diameter of ultrafast **9r9-PBI** (26.7 Å) lies between that of **rr8-** (26.4 Å) and **rr9-PBI** (27.0 Å), suggesting that this diameter falls within a particularly preferable range accessible only to hybrids of **r** with *n*-octyl and *n*-nonyl chains. In all cases, the intracolumnar π–π distance is 3.7 Å.

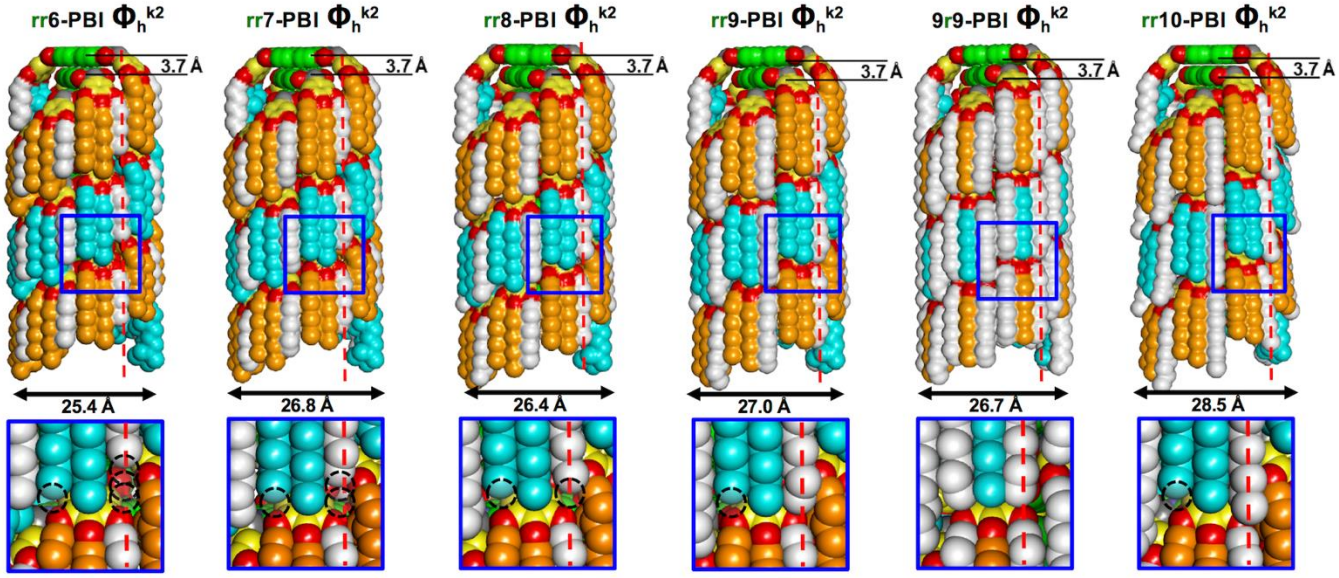

Figure 5. Models of the cogwheel columns of $\mathbf{\Phi_h^{k2}}$ self-organized from **rr6-**, **rr7-**, **rr8-**, **rr9-**, **9r9-**, and **rr10-PBI**. Intramolecular spacing and column diameter are indicated. Insets illustrate the space filling by the alkyl ends from the 3- and 5- positions of the dendron as a function of their length and sequence. Dashed circles in insets indicate empty space on the column periphery.

One of the key requirements of the cogwheel model (Figure 1d) is the alkyl chain coat length being almost equal to the helical half-pitch of 14.8 Å (= 4 × 3.7 Å). Both previous studies of the cogwheel model have utilized homochiral dm8*[18] or dm8* (**r**)-*n*-octyl hybrids,[19] with a linear length of 8 carbons. This length forms a coat that almost covers the entire column periphery, leaving small gaps between the end of the alkyl chains of the *i*th molecule without steric hindrance from the (*i* + 4)th molecule in the column (see inset for **rr8-PBI** in Figure 5). Shorter alkyl chains do not adequately cover the column exterior (see inset for **rr6-PBI** and dashed circular marks denoting empty space in Figure 5) whereas longer alkyl chains lead to steric hindrance and an unfavorable tilting of the alkyl chain away from the column axis (such as for **rr10-PBI**). The small degree of unoccupied space in **r**/*n*-octyl hybrids is sufficient to accommodate a 9th carbon in the alkyl chain without significant steric penalties; hence **rr9-** and especially **9r9-PBI** most

efficiently fill the column periphery with aliphatic chains. A close inspection of the structures of the cogwheel columns of **rr9-** and **9r9-PBI** (Figure 5) demonstrates a perfect tertiary structure for **9r9-PBI** assembly and a small imperfection in the column derived from **rr9-PBI** (see dashed circle in the 3-position) due to the shorter **r** group at the 3-position of the dendron. Therefore, the ideal place for the **r** group is in 4-position of the dendron while the ideal places for the **9** groups are in the 3- and 5-positions. This conclusion is also supported by solid state NMR experiments to be discussed in a later subsection. The $\mathbf{\Phi_h^{k1}}$-$\mathbf{\Phi_h^{k2}}$ transitions are observed on heating and cooling for **9r9-PBI** and are present irrespective of the heating and cooling rate (Figure 3b). However, **rr9-PBI** assembly does not show the first order transition on cooling at 107 °C that **9r9-PBI** assembly shows (Figure 2) upon cooling at 10 ^{o}C/min. It is tempting to attribute such observations to the perfect **9r9-PBI** sequence that provides the ideal tertiary structure. However, DSC studies of **rr9-PBI** and **9r9-PBI** (Figure 2) provide near-identical $\mathbf{\Phi_h^{k1}}$-$\mathbf{\Phi_h^{k2}}$ transition temperatures (136 and 137 °C, respectively) and enthalpies (1.40 and 1.42 kcal/mol) upon heating, suggesting that the thermodynamic driving force for $\mathbf{\Phi_h^{k2}}$ formation is very close for **rr9-PBI** and **9r9-PBI**. Since the rate of formation of the $\mathbf{\Phi_h^{k2}}$ phase transition is almost independent of the heating and cooling rate (Figure 3 and Figure 4) we can conclude that the formation of cogwheel assembly in **9r9-PBI** is extraordinarily accelerated *vs* that of **rr9-PBI**, and all other sequence-defined assemblies, although both assemblies have almost identical thermodynamic driving forces (*vide infra*, Figure 2). *Hence the observed difference in the rate of* $\boldsymbol{\Phi_h^{k2}}$ *formation must be due to kinetic effects*.

We propose that the $\mathbf{\Phi_h^{k1}}$–$\mathbf{\Phi_h^{k2}}$ transition is so fast in **9r9-PBI** because there are many more local fluctuations of the favorable cogwheel $\mathbf{\Phi_h^{k2}}$ structure within the $\mathbf{\Phi_h^{k1}}$ phase below, and perhaps even above, the transition temperature, compared to **rr9-PBI**. Due to the increased degree of branching in **rr9-PBI**, such fluctuations are expected to have higher free energy and thus are less favorable. This is linked to the higher entropy that involves disorder, and hence mobility, of the linear chains compared to branched

ones.[30] More $\mathbf{\Phi_h^{k2}}$ fluctuations increase the probability that a fluctuation reaches critical nucleus size, thereby dramatically accelerating the nucleation of the $\mathbf{\Phi_h^{k2}}$ and leading to an extraordinarily accelerated rate of self-organization and crystallization. The lack of cogwheel phases in PBIs dendronized with all *n*-alkyl chains[20c] suggests that the methyl branch of the **r** chain is required for cogwheel packing, and the ideal length and position of the *n*-nonyl chains in **9r9-PBI** unpredictably lead to the formation of the cogwheel phase being kinetically accessible even at very fast heating and cooling rates.

Solid State NMR Probes Distribution of Local Chain Conformations and Molecular Fluctuations. The formation of columnar arrays with long-range order is not only affected by the π–π stacking of the PBI cores, but also by the local conformations of the aliphatic side chains, in particular if the volume locally available for molecular fluctuations changes in amount or shape. Solid state ^{13}C NMR chemical shifts are very sensitive to local intracolumnar packing arrangements, acting as probes for local conformational distributions[12] and thus nicely augmenting the information available from XRD and DSC. ^{13}C cross-polarization magic angle spinning (CP-MAS) experiments on hybrid PBIs with **r**/*n*-nonyl dendrons show that the conformational distribution is largely determined by the attachment site at the phenyl ring (Figure 6).

Dimethyloctyl (**r**) chains in the 3- and 5-positions (Figure 6a) show a broad chemical shift distribution resulting from a broad conformational distribution of the CH_2 groups next to the chiral center (green) and the chiral methyl group (yellow), whereas **r** chains in the 4-position (**9r9-PBI** spectrum in Figure 6b) exhibit sharp peaks for those sites. The narrower conformational distribution of 4- vs 3- or 5-**r** chains is hardly affected by neighboring chains (Figure 6b), general for all hybrid **r**/*n*-alkyl dendrons with n = 6–10 (Figure S60), and invariant to temperature (Figure S61). In addition, the sum spectrum of **9r9-** and **99r-PBI** (broken red line, Figure 6b) is significantly narrower in the region of the chiral methyl group (green) than **rr9-PBI** (solid black line). This suggests a higher local mobility of the chiral methyl groups

in **9r9-** and **99r-PBI**, more efficiently averaging different packing arrangements of the methyl group within the supramolecular column. This higher local mobility may be aided by the presence of two, more dynamic, linear *n*-nonyl chains in **9r9-** and **99r-PBI** compared to the single *n*-nonyl chain in **rr9-PBI**.

General Design Principles for Cogwheel Assembly Beyond the Current System. The discovery of ultrafast cogwheel assembly for **9r9-PBI** enhances our understanding of the role of alkyl chain design in the cogwheel mechanism of self-assembly. This mechanism provides a route to highly ordered arrays of homochiral helical supramolecular columns irrespective of molecular chirality, a structure of potential interest for numerous applications and fundamental studies on complex systems. To date this model has been demonstrated only with dendronized PBIs, but cogwheel assembly is applicable to a broader range of molecular cores.

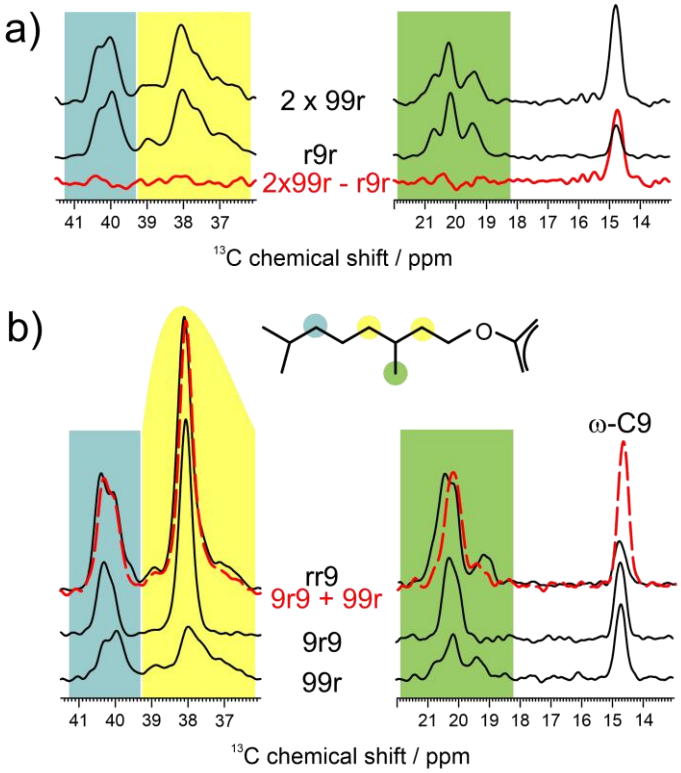

Figure 6. ^{13}C CP-MAS NMR spectra of hybrid PBIs with dm8*/*n*-nonyl dendrons. (a) The NMR spectra of **99r-** and **r9r-PBI** differ only at the 14.7 ppm signal assigned to the chain end of the linear *n*-nonyl chains, as seen in the red difference spectrum. (b) Superimposing the NMR spectra of dm8* chains in *meta*- (**99r-PBI**) and *para*-position (**9r9-PBI**) provides the NMR spectrum for **rr9-PBI** for the main chain sites (yellow and blue). Green region denotes chiral methyl group.

To facilitate this process, we propose three criteria that must be satisfied for cogwheel assembly (Figure 7). The acceleration of cogwheel formation for **9r9-PBI** demonstrates that complete space-filling is needed to achieve the kinetically most favorable crystallization. First, the length of the alkyl chain coat jacketing the supramolecular column must match the helical half-pitch and, most preferably, completely fill all available space on the column exterior. Molecules of **9r9-PBI** are stacked with a π–π distance of 3.6 Å, giving a helical half-pitch of 14.4 Å (= 4 × 3.6 Å, Figure 7a). The shortest distance for close-contact planar aromatic cores is 3.3 Å[31] (i.e., helical-half pitch of 13.2 Å), corresponding to an ideal alkyl chain length of between 7 and 8 carbons (Figure 7a). In contrast, increasing the spacing between aromatic cores, such as with non-planar 1,6,7,12-tetrachloroperylene bisimide (Cl_4-PBI),[32] would require a longer alkyl chain to cover the column exterior.

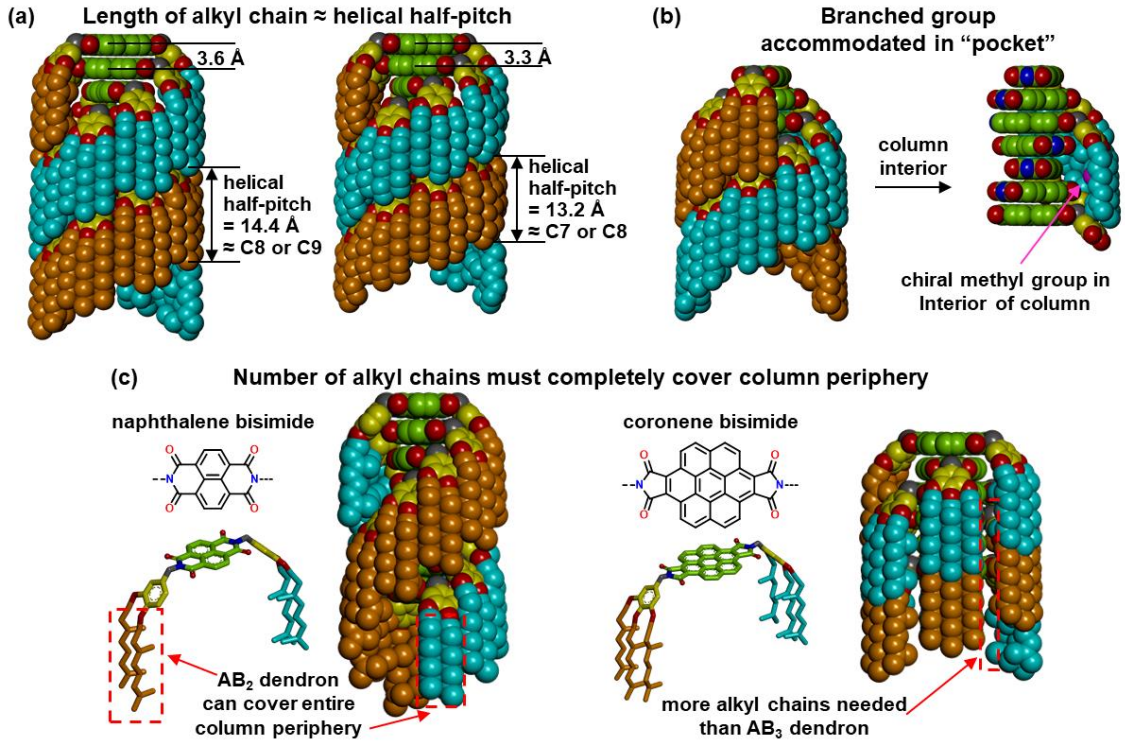

Figure 7. Design principles for the translation of the cogwheel model to other systems. (a) The length of the alkyl chain must match the helical half-pitch, which is dictated by intermolecular π–π stacking distance. (b) There must be a "pocket" of available space in which the branch group (i.e. a chiral methyl group in dm8*) can be accommodated. (c) The alkyl chain jacket on the column periphery must be continuous. (left) Cores smaller than PBI, e.g. naphthalene bisimide, need fewer alkyl chains for complete jacketing, whereas (right) cores larger than PBI, e.g. coronene bisimide, need more alkyl chains.

The second criterion, established previously,[19] is that the minidendron must contain at least one branched alkyl chain to prevent column interdigitation with alkyl tails being perpendicular rather than parallel to the long axis of the column. The methyl branch in **9r9-PBI** is accommodated jn a pocket defined by adjacent PBIs in the supramolecular column (Figure 7b). Most likely, the cogwheel model will tolerate alternative branching point positions, if space is available to accommodate the chiral group without disrupting the column periphery. Geometric considerations suggest that the methyl group should be closer to the dendron phenyl ring rather than the free end of the alkyl chain.

Finally, the number of alkyl chains must be modified to fill the entire periphery of the column for different core sizes, to account for differences in column diameter and intermolecular rotation. This intermolecular rotation, and thus helical pitch, will vary depending on size and shape of the aromatic core; for the current PBIs, 45° is favorable (Figure 1b). A compound with a different aromatic core may have a different minimum energy rotation angle that would favor a helix with a different pitch. It is then necessary to match both the length and the number of the pendant chains to the half-pitch of that helix. For example (Figure 7c), smaller cores (e.g. naphthalene bisimide,[33] NBI) may require fewer, longer alkyl chains than **9r9-PBI**, whereas larger cores (e.g. coronenes[34]) may require more, potentially shorter chains. Dendrons provide a particularly powerful tool to precisely modulate alkyl chain number and length, ranging from AB_2 to AB_5 in a single dendron generation.[35] Higher numbers of alkyl chains may require multi-generation dendron designs[22a–d] or new methodologies to program first degeneration AB_n self-assembling dendrons with *n* larger than 3.

CONCLUSIONS

Taken together, the combination of DSC, XRD, and solid state NMR presented here suggest that the extraordinary acceleration of the self-organization of the cogwheel $\mathbf{\Phi_h^{k2}}$ phase in **9r9-PBI** is a result of both favorable crystal packing and local chain dynamics. The results show that even just one branched

chain out of three on a dendron is sufficient to disfavor intercolumnar interdigitation and instead favor axial chain alignment. The second condition for cogwheel assembly is matching the chain length to the half-pitch length of the helix. DSC and XRD (Figures 2–4 and S49–S57) suggest that the optimal chain length satisfying this condition is 8 and especially 9 carbons. More specifically, molecular modeling and reconstruction of fiber XRD by molecular models (Figures 4 and 5) indicate that the periphery of the supramolecular column is incompletely filled by linear and branched octyl chains, but that incorporation of *n*-nonyl chains can be tolerated and leads to better occupation of the aliphatic column periphery. Hence a mixture of **r** and **9** best in 9r9 sequence is most favorable for filling space within the crystalline assemblies of the cogwheel $\mathbf{\Phi_h^{k2}}$ phase. Solid state NMR (Figure 6) has further demonstrated a higher mobility of linear compared to the branched chains, supporting the increased $\mathbf{\Phi_h^{k1}}$-$\mathbf{\Phi_h^{k2}}$ transition rate of **9r9-** and **99r-PBI** compared to that of **rr9-** and **r9r-PBI**. NMR results also show that the presence of a **r** chain in the 4-position of the (3,4,5)-minidendron experiences a narrower distribution of conformations within the columnar array, likely indicating that the tertiary structure necessary for the cogwheel model is preferentially accessible to dendrons with 4-**r** substitution. Therefore, the **9r9**-sequence represents the ideal dendron to cover the column periphery, enabling rapid formation of the highly ordered $\mathbf{\Phi_h^{k2}}$ crystal. *To the best of our knowledge the formation of the* $\boldsymbol{\Phi_h^{k2}}$ *crystal represents the fastest self-organizing and crystallizing supramolecular or covalent natural or synthetic macromolecule known to date.* This substantial acceleration in self-organization could not be predicted, neither from our previous knowledge of the cogwheel model nor from our preliminary experiments reported in the previous communication.[19] These insights provide design guidelines for highly ordered, self-healing, and rapidly forming columnar structures, properties that are highly desirable in stable, fast-switching, fast-forming and thermoresponsive defect-free functional materials. The methodology described here, relying on not just XRD but also DSC and solid state NMR, may bring new insights for other complex soft matter.[36] Indeed, the presently

employed *n*-semiconducting PBI core[16] is only one option (Figure 7), replaceable with other core moieties forming similar $\mathbf{\Phi_h^{k2}}$-type structures. The precise design of aliphatic chains may have relevance not just for the directed supramolecular assembly of columnar assemblies, but also for even more complex assemblies self-organized from spheres such as the Frank-Kasper phases assembled from supramolecular dendrimers and from self-organizable dendronized polymers,[37] and as synthetic cells generated from amphiphilic including sequence-defined Janus-dendrimers and Janus-glycodendrimers.[24,38]

AUTHOR INFORMATION

Corresponding Author

percec@sas.upenn.edu

Present Addresses

□B.E.P.: Department of Chemistry and International Institute of Nanotechnology, Northwestern University, Evanston, Illinois 60208, United States.

Notes

The authors declare no competing financial interests.

Supporting Information

Experimental methods, synthetic procedures with complete characterization data, structural and thermal analysis parameters, additional DSC, XRD and solid state NMR data and associated discussion

ACKNOWLEDGMENTS

Financial support by the National Science Foundation (DMR-1066116 and DMR-1807127 (V.P.), DMR-1120901 (V.P. and P.A.H.)), the Humboldt Foundation (V.P.) and the P. Roy Vagelos Chair at Penn (V.P.) is gratefully acknowledged. B.E.P. thanks the Howard Hughes Medical Institute for an International Student Research Fellowship. We also thank Professor Paul A. Heiney from the Department of Physics and Astronomy, University of Pennsylvania for helpful discussions concerning the X-ray experiments.

REFERENCES

(1) (a) Nanda, V.; Andrianarijaona, A.; Narayanan, C. The Role of Protein Homochirality in Shaping the Energy Landscape of Folding. *Protein Sci.* **2007**, *16*, 1667–1675. (b) Chen, Z.; Lichtor, P. A.; Berliner, A. P.; Chen, J. C.; Liu, D. R. Evolution of Sequence-Defined Highly Functionalized Nucleic Acid Polymers. *Nat. Chem.* **2018**, *10*, 420–427. (c) Cecconello, A.; Simmel, F. C. Controlling Chirality across Length Scales Using DNA. *Small* **2019**, *15*, 1805419.

(2) (a) Watson, J. D.; Crick, F. H. C. Molecular Structure of Nucleic Acids: A Structure for Deoxyribose Nucleic Acid. *Nature* **1953**, *171*, 737–738. (b) Sarko, A.; Marchessault, R. H. Crystal Structure of Amylose Triacetate: A Nonintegral Helix. *Science* **1966**, *154*, 1658–1659.

(3) (a) Frank, P.; Bonner, W. A.; Zare, R. N. On One Hand But Not The Other: The Challenge of the Origin and Survival of Homochirality in Prebiotic Chemistry. In *Chemistry for the 21st Century*; Wiley-VCH Verlag GmbH, 2000; pp 175–208. (b) Weissbuch, I.; Lahav, M. Crystalline Architectures as Templates of Relevance to the Origins of Homochirality. *Chem. Rev.* **2011**, *111*, 3236–3267. (c) Percec, V.; Leowanawat, P. Why Are Biological Systems Homochiral? *Isr. J. Chem.* **2011**, *51*, 1107–1117. (d) Hein, J. E.; Gherase, D.; Blackmond, D. G. Chemical and Physical Models for the Emergence of Biological Homochirality. In *Biochirality*; Cintas, P., Ed.; Topics in Current Chemistry; Springer Berlin Heidelberg, 2013; Vol. 333, pp 83–108.

(4) (a) Soai, K.; Matsumoto, A. Asymmetric Autocatalysis and the Origin of Homochirality. In *Stereochemistry and Global Connectivity: The Legacy of Ernest L. Eliel Volume 2*; ACS Symposium Series; American Chemical Society, 2017; Vol. 1258, pp 3–27. (b) Hawbaker, N. A.; Blackmond, D. G. Rationalization of Asymmetric Amplification *via* Autocatalysis Triggered by Isotopically Chiral Molecules. *ACS Cent. Sci.* **2018**, *4*, 776–780. (c) Blackmond, D. G. Autocatalytic Models for the Origin of Biological Homochirality. *Chem. Rev.* **2019**, *ASAP*. DOI: 10.1021/acs.chemrev.9b00557.

(5) (a) Toxvaerd, S. Origin of Homochirality in Biological Systems. *Int. J. Astrobiol.* **2005**, *4*, 43–48. (b) Sisco, S. W.; Moore, J. S. Homochiral Self-Sorting of BINOL Macrocycles. *Chem. Sci.* **2014**, *5*, 81–85.

(6) Pasteur, L. On the Relations That Can Exist between Crystalline Form, and Chemical Composition, and the Sense of Rotary Polarization. *Ann. Chim. Phys.* **1848**, *24*, 442–459.

(7) (a) Percec, V.; Heck, J.; Johansson, G.; Tomazos, D.; Kawasumi, M.; Ungar, G. Molecular-Recognition-Directed Self-Assembly of Supramolecular Polymers. *J. Macromol. Sci., Part A: Pure Appl. Chem.* **1994**, *31*, 1031–1070. (b) Lehn, J.-M. Supramolecular Polymer Chemistry–Scope and Perspectives. *Polym. Int.* **2002**, *51*, 825–839. (c) Lehn, J.-M. Dynamers: Dynamic Molecular and Supramolecular Polymers. *Prog. Polym. Sci.* **2005**, *30*, 814–831. (d) de Greef, T. F. A.; Smulders, M. M. J.; Wolffs, M.; Schenning, A. P. H. J.; Sijbesma, R. P.; Meijer, E. W. Supramolecular Polymerization. *Chem. Rev.* **2009**, *109*, 5687–5754. (e) Aida, T.; Meijer, E. W. Supramolecular Polymers – We've Come Full Circle. *Isr. J. Chem.* **2020**, *60*, 33–47.

(8) (a) Pokroy, B.; Kang, S. H.; Mahadevan, L.; Aizenberg, J. Self-Organization of a Mesoscale Bristle into Ordered, Hierarchical Helical Assemblies. *Science* **2009**, *323*, 237–240. (b) Yashima, E.; Ousaka, N.; Taura, D.; Shimomura, K.; Ikai, T.; Maeda, K. Supramolecular Helical Systems: Helical Assemblies of Small Molecules, Foldamers, and Polymers with Chiral Amplification and Their Functions. *Chem. Rev.* **2016**, *116*, 13752–13990.

(9) (a) Chen, J.; Leung, F. K.-C.; Stuart, M. C. A.; Kajitani, T.; Fukushima, T.; van der Giessen, E.; Feringa, B. L. Artificial Muscle-like Function from Hierarchical Supramolecular Assembly of Photoresponsive Molecular Motors. *Nat. Chem.* **2017**, *10*, 132–138. (b) Hendricks, M. P.; Sato,

K.; Palmer, L. C.; Stupp, S. I. Supramolecular Assembly of Peptide Amphiphiles. *Acc. Chem. Res.* **2017**, *50*, 2440–2448.

(10) (a) Sato, K.; Itoh, Y.; Aida, T. Homochiral Supramolecular Polymerization of Bowl-Shaped Chiral Macrocycles in Solution. *Chem. Sci.* **2014**, *5*, 136–140. (b) Zhao, D.; van Leeuwen, T.; Cheng, J.; Feringa, B. L. Dynamic Control of Chirality and Self-Assembly of Double-Stranded Helicates with Light. *Nat. Chem.* **2016**, *9*, 250–256. (c) Venkata Rao, K.; Miyajima, D.; Nihonyanagi, A.; Aida, T. Thermally Bisignate Supramolecular Polymerization. *Nat. Chem.* **2017**, *9*, 1133–1139.

(11) Roche, C.; Sun, H.-J.; Prendergast, M. E.; Leowanawat, P.; Partridge, B. E.; Heiney, P. A.; Araoka, F.; Graf, R.; Spiess, H. W.; Zeng, X.; Ungar, G.; Percec, V. Homochiral Columns Constructed by Chiral Self-Sorting during Supramolecular Helical Organization of Hat-Shaped Molecules. *J. Am. Chem. Soc.* **2014**, *136*, 7169–7185.

(12) (a) Hansen, M. R.; Graf, R.; Spiess, H. W. Solid-State NMR in Macromolecular Systems: Insights on How Molecular Entities Move. *Acc. Chem. Res.* **2013**, *46*, 1996–2007. (b) Hansen, M. R.; Graf, R.; Spiess, H. W. Interplay of Structure and Dynamics in Functional Macromolecular and Supramolecular Systems As Revealed by Magnetic Resonance Spectroscopy. *Chem. Rev.* **2016**, *116*, 1272–1308. (c) Tonelli, A. E. Polymer Microstructure: The Conformational Connection to NMR. In *Modern Magnetic Resonance*; Webb, G. A., Ed.; Springer Netherlands: Dordrecht, 2006; pp 567–574.

(13) (a) Percec, V.; Dulcey, A. E.; Balagurusamy, V. S. K.; Miura, Y.; Smidrkal, J.; Peterca, M.; Nummelin, S.; Edlund, U.; Hudson, S. D.; Heiney, P. A.; Duan, H.; Magonov, S. N.; Vinogradov, S. A. Self-Assembly of Amphiphilic Dendritic Dipeptides into Helical Pores. *Nature* **2004**, *430*, 764–768. (b) Percec, V.; Dulcey, A. E.; Peterca, M.; Ilies, M.; Ladislaw, J.; Rosen, B. M.; Edlund, U.; Heiney, P. A. The Internal Structure of Helical Pores Self-Assembled from Dendritic Dipeptides Is Stereochemically Programmed and Allosterically Regulated. *Angew. Chem. Int. Ed.* **2005**, *44*, 6516–6521. (c) Rosen, B. M.; Peterca, M.; Morimitsu, K.; Dulcey, A. E.; Leowanawat, P.; Resmerita, A.-M.; Imam, M. R.; Percec, V. Programming the Supramolecular Helical Polymerization of Dendritic Dipeptides *via* the Stereochemical Information of the Dipeptide. *J. Am. Chem. Soc.* **2011**, *133*, 5135–5151.

(14) Rosen, B. M.; Roche, C.; Percec, V. Self-Assembly of Dendritic Dipeptides as a Model of Chiral Selection in Primitive Biological Systems. *Top. Curr. Chem.* **2013**, *333*, 213–253.

(15) Natta, G.; Pino, P.; Corradini, P.; Danusso, F.; Moraglio, G.; Mantica, E.; Mazzanti, G. Crystalline High Polymers of α-Olefins. *J. Am. Chem. Soc.* **1955**, *77*, 1708–1710.

(16) (a) Huang, C.; Barlow, S.; Marder, S. R. Perylene-3,4,9,10-Tetracarboxylic Acid Diimides: Synthesis, Physical Properties, and Use in Organic Electronics. *J. Org. Chem.* **2011**, *76*, 2386–2407. (b) Zhan, X.; Facchetti, A.; Barlow, S.; Marks, T. J.; Ratner, M. A.; Wasielewski, M. R.; Marder, S. R. Rylene and Related Diimides for Organic Electronics. *Adv. Mater.* **2011**, *23*, 268–284. (c) Würthner, F.; Saha-Möller, C. R.; Fimmel, B.; Ogi, S.; Leowanawat, P.; Schmidt, D. Perylene Bisimide Dye Assemblies as Archetype Functional Supramolecular Materials. *Chem. Rev.* **2016**, *116*, 962–1052. (d) Krieg, E.; Niazov-Elkan, A.; Cohen, E.; Tsarfati, Y.; Rybtchinski, B. Noncovalent Aqua Materials Based on Perylene Diimides. *Acc. Chem. Res.* **2019**, *52*, 2634–2646.

(17) (a) Tomalia, D. A.; Fréchet, J. M. J. Discovery of Dendrimers and Dendritic Polymers: A Brief Historical Perspective. *J. Polym. Sci. Part A: Polym. Chem.* **2002**, *40*, 2719–2728. (b) Fréchet, J. M. J. Dendrimers and Supramolecular Chemistry. *Proc. Natl. Acad. Sci. U. S. A.* **2002**, *99*, 4782–4787. (c) Rosen, B. M.; Wilson, C. J.; Wilson, D. A.; Peterca, M.; Imam, M. R.; Percec, V. Dendron-Mediated Self-Assembly, Disassembly, and Self-Organization of Complex Systems. *Chem. Rev.* **2009**, *109*, 6275–6540. (d) Sun, H.-J.; Zhang, S.; Percec, V. From Structure to

Function *via* Complex Supramolecular Dendrimer Systems. *Chem. Soc. Rev.* **2015**, *44*, 3900–3923. (e) Tomalia, D. A.; Khanna, S. V. A Systematic Framework and Nanoperiodic Concept for Unifying Nanoscience: Hard/Soft Nanoelements, Superatoms, Meta-Atoms, New Emerging Properties, Periodic Property Patterns, and Predictive Mendeleev-like Nanoperiodic Tables. *Chem. Rev.* **2016**, *116*, 2705–2774. (f) Percec, V. Merging Macromolecular and Supramolecular Chemistry into Bioinspired Synthesis of Complex Systems. *Isr. J. Chem.* **2020**, *60*, 48–66.

(18) Roche, C.; Sun, H.-J.; Leowanawat, P.; Araoka, F.; Partridge, B. E.; Peterca, M.; Wilson, D. A.; Prendergast, M. E.; Heiney, P. A.; Graf, R.; Spiess, H. W.; Zeng, X.; Ungar, G.; Percec, V. A Supramolecular Helix That Disregards Chirality. *Nat. Chem.* **2016**, *8*, 80–89.

(19) Partridge, B. E.; Wang, L.; Sahoo, D.; Olsen, J. T.; Leowanawat, P.; Roche, C.; Ferreira, H.; Reilly, K. J.; Zeng, X.; Ungar, G.; Heiney, P. A.; Graf, R.; Spiess, H. W.; Percec, V. Sequence-Defined Dendrons Dictate Supramolecular Cogwheel Assembly of Dendronized Perylene Bisimides. *J. Am. Chem. Soc.* **2019**, *141*, 15761–15766.

(20) (a) Percec, V.; Peterca, M.; Tadjiev, T.; Zeng, X.; Ungar, G.; Leowanawat, P.; Aqad, E.; Imam, M. R.; Rosen, B. M.; Akbey, U.; Graf, R.; Sekharan, S.; Sebastiani, D.; Spiess, H. W.; Heiney, P. A.; Hudson, S. D. Self-Assembly of Dendronized Perylene Bisimides into Complex Helical Columns. *J. Am. Chem. Soc.* **2011**, *133*, 12197–12219. (b) Percec, V.; Hudson, S. D.; Peterca, M.; Leowanawat, P.; Aqad, E.; Graf, R.; Spiess, H. W.; Zeng, X.; Ungar, G.; Heiney, P. A. Self-Repairing Complex Helical Columns Generated *via* Kinetically Controlled Self-Assembly of Dendronized Perylene Bisimides. *J. Am. Chem. Soc.* **2011**, *133*, 18479–18494. (c) Percec, V.; Sun, H.-J.; Leowanawat, P.; Peterca, M.; Graf, R.; Spiess, H. W.; Zeng, X.; Ungar, G.; Heiney, P. A. Transformation from Kinetically into Thermodynamically Controlled Self-Organization of Complex Helical Columns with 3D Periodicity Assembled from Dendronized Perylene Bisimides. *J. Am. Chem. Soc.* **2013**, *135*, 4129–4148.

(21) Li, Y.; Lin, S.; Goddard, W. A. Efficiency of Various Lattices from Hard Ball to Soft Ball: Theoretical Study of Thermodynamic Properties of Dendrimer Liquid Crystal from Atomistic Simulation. *J. Am. Chem. Soc.* **2004**, *126*, 1872–1885.

(22) (a) Percec, V.; Cho, W.-D.; Ungar, G.; Yeardley, D. J. P. Synthesis and Structural Analysis of Two Constitutional Isomeric Libraries of AB_2-Based Monodendrons and Supramolecular Dendrimers. *J. Am. Chem. Soc.* **2001**, *123*, 1302–1315. (b) Percec, V.; Peterca, M.; Sienkowska, M. J.; Ilies, M. A.; Aqad, E.; Smidrkal, J.; Heiney, P. A. Synthesis and Retrostructural Analysis of Libraries of AB_3 and Constitutional Isomeric AB_2 Phenylpropyl Ether-Based Supramolecular Dendrimers. *J. Am. Chem. Soc.* **2006**, *128*, 3324–3334. (c) Rosen, B. M.; Wilson, D. A.; Wilson, C. J.; Peterca, M.; Won, B. C.; Huang, C.; Lipski, L. R.; Zeng, X.; Ungar, G.; Heiney, P. A.; Percec, V. Predicting the Structure of Supramolecular Dendrimers *via* the Analysis of Libraries of AB_3 and Constitutional Isomeric AB_2 Biphenylpropyl Ether Self-Assembling Dendrons. *J. Am. Chem. Soc.* **2009**, *131*, 17500−17521. (d) Zhang, S.; Sun, H.-J.; Hughes, A. D.; Moussodia, R.-O.; Bertin, A.; Chen, Y.; Pochan, D. J.; Heiney, P. A.; Klein, M. L.; Percec, V. Self-Assembly of Amphiphilic Janus Dendrimers into Uniform Onion-Like Dendrimersomes with Predictable Size and Number of Bilayers. *Proc. Natl. Acad. Sci. U. S. A.* **2014**, *111*, 9058–9063. (e) Bradford, V. J.; Iverson, B. L. Amyloid-like Behavior in Abiotic, Amphiphilic Foldamers. *J. Am. Chem. Soc.* **2008**, *130*, 1517–1524. (f) Wang, Y.; Kaur, K.; Scannelli, S. J.; Bitton, R.; Matson, J. B. Self-Assembled Nanostructures Regulate H_2S Release from Constitutionally Isomeric Peptides. *J. Am. Chem. Soc.* **2018**, *140*, 14945–14951. (g) Lin, Z.; Yang, X.; Xu, H.; Sakurai, T.; Matsuda, W.; Seki, S.; Zhou, Y.; Sun, J.; Wu, K.-Y.; Yan, X.-Y.; Zhang, R.; Huang, M.; Mao, J.; Wesdemiotis, C.; Aida, T.; Zhang, W.; Cheng, S. Z. D. Topologically Directed Assemblies of Semiconducting Sphere–Rod

Conjugates. *J. Am. Chem. Soc.* **2017**, *139*, 18616–18622. (h) Yan, X.-Y.; Lin, Z.; Zhang, W.; Xu, H.; Guo, Q.-Y.; Liu, Y.; Luo, J.; Liu, X.-Y.; Zhang, R.; Huang, J.; Liu, T.; Su, Z.; Zhang, R.; Zhang, S.; Liu, T.; Cheng, S. Z. D. Magnifying the Structural Components of Biomembranes: A Prototype for the Study of the Self-Assembly of Giant Lipids. *Angew. Chem. Int. Ed.* **2020**, *59*, 5226–5234.

(23) (a) Tomalia, D. A.; Naylor, A. M.; Goddard W. A. Starburst Dendrimers: Molecular-Level Control of Size, Shape, Surface Chemistry, Topology and Flexibility from Atom to Macroscopic Matter. *Angew. Chem. Int. Ed.* **1990**, *29*, 138–175. (b) Hawker, C. J.; Frechet, J. M. J. Preparation of Polymers with Controlled Molecular Architecture. A New Convergent Approach to Dendritic Macromolecules. *J. Am. Chem. Soc.* **1990**, *112*, 7638–7647. (c) Edwardson, T. G. W.; Carneiro, K. M. M.; Serpell, C. J.; Sleiman, H. F. An Efficient and Modular Route to Sequence-Defined Polymers Appended to DNA. *Angew. Chem. Int. Ed.* **2014**, *53*, 4567–4571. (d) Hamblin, G. D.; Rahbani, J. F.; Sleiman, H. F. Sequential Growth of Long DNA Strands with User-Defined Patterns for Nanostructures and Scaffolds. *Nat. Commun.* **2015**, *6*, 7065. (e) Leibfarth, F. A.; Johnson, J. A.; Jamison, T. F. Scalable Synthesis of Sequence-Defined Unimolecular Macromolecules by Flow-IEG. *Proc. Natl. Acad. Sci. U. S. A.* **2015**, *112*, 10617–10622. (f) Xu, J.; Fu, C.; Shanmugam, S.; Hawker, C. J.; Moad, G.; Boyer, C. Synthesis of Discrete Oligomers by Sequential PET-RAFT Single-Unit Monomer Insertion. *Angew. Chem. Int. Ed.* **2017**, *56*, 8376-8383. (g) Dong, R.; Liu, R.; Gaffney, P. R. J.; Schaepertoens, M.; Marchetti, P.; Williams, C. R.; Chen, R.; Livingston, A. G. Sequence-Defined Multifunctional Polyethers *via* Liquid-Phase Synthesis with Molecular Sieving. *Nat. Chem.* **2019**, *11*, 136–145. (h) Yue, K.; Huang, M.; Marson, R. L.; He, J.; Huang, J.; Zhou, Z.; Wang, J.; Liu, C.; Yan, X.; Wu, K.; Guo, Z.; Liu, H.; Zhang, W.; Ni, P.; Wesdemiotis, C.; Zhang, W.-B.; Glotzer, S. C.; Cheng, S. Z. D. Geometry Induced Sequence of Nanoscale Frank–Kasper and Quasicrystal Mesophases in Giant Surfactants. *Proc. Natl. Acad. Sci. U.S.A.* **2016**, *113*, 14195–14200. (i) Zhang, W.; Lu, X.; Mao, J.; Hsu, C.-H.; Mu, G.; Huang, M.; Guo, Q.; Liu, H.; Wesdemiotis, C.; Li, T.; Zhang, W.-B.; Li, Y.; Cheng S. Z. D. Sequence-Mandated, Distinct Assembly of Giant Molecules. *Angew. Chem. Int. Ed.* **2017**, *56*, 15014–15019. (j) Ni, B.; Qu, H.; Mao, J.; Bai, R.; Zhang, S.; Feng, X.; Wesdemiotis, C.; Dong, X.-H.; Cheng, S. Z. D. Facile Synthesis and Linker Guided Self-Assembly of Dendron-Like Amphiphiles. *Polymer* **2019**, *167*, 118–121. (k) Zhang, R.; Feng, X.; Zhang, R.; Shan, W.; Su, Z.; Mao, J.; Wesdemiotis, C.; Huang, J.; Yan, X.-Y.; Liu, T.; Li, T.; Huang, M.; Lin, Z.; Shi, A.-C.; Cheng, S. Z. D. Breaking Parallel Orientation of Rods *via* a Dendritic Architecture toward Diverse Supramolecular Structures. *Angew. Chem. Int. Ed.* **2019**, *58*, 11879–11885.

(24) (a) Zuckermann, R. N.; Kerr, J. M.; Kent, S. B. H.; Moos, W. H. Efficient Method for the Preparation of Peptoids [Oligo(*N*-substituted Glycines]) by Submonomer Solid-Phase Synthesis. *J. Am. Chem. Soc.* **1992**, *114*, 10646–10647. (b) Caruthers, M. H. Gene Synthesis Machines: DNA Chemistry and Its Uses. *Science* **1985**, *230*, 281–285. (c) Caruthers, M. H. The Chemical Synthesis of DNA/RNA: Our Gift to Science. *J. Biol. Chem.* **2013**, *288*, 1420–1427. (d) Plante, O. J.; Palmacci, E. R; Seeberger, P. H. Automated Solid-Phase Synthesis of Oligosaccharides. *Science* **2001**, *291*, 1523–1527. (e) Guberman, M.; Seeberger, P. H. Automated Glycan Assembly: A Perspective. *J. Am. Chem. Soc.* **2019**, *141*, 5581–5592.

(25) (a) Zhang, S.; Xiao, Q.; Sherman, S. E.; Muncan, A.; Ramos Vicente, A. D. M.; Wang, Z.; Hammer, D. A.; Williams, D.; Chen, Y.; Pochan, D. J.; Vértesy, S.; André, S.; Klein, M. L.; Gabius, H.-J.; Percec, V. Glycodendrimersomes from Sequence-Defined Janus Glycodendrimers Reveal High Activity and Sensor Capacity for the Agglutination by Natural Variants of Human Lectins. *J. Am. Chem. Soc.* **2015**, *137*, 13334–13344. (b) Xiao, Q.; Zhang, S.; Wang, Z.; Sherman, S. E.;

Moussodia, R.-O.; Peterca, M.; Muncan, A.; Williams, D. R.; Hammer, D. A.; Vértesy, S.; André, S.; Gabius, H.-J.; Klein, M. L.; Percec, V. Onion-like Glycodendrimersomes from Sequence-Defined Janus Glycodendrimers and Influence of Architecture on Reactivity to a Lectin. *Proc. Natl. Acad. Sci. U. S. A.* **2016**, *113*, 1162–1167. (c) Kopitz, J.; Xiao, Q.; Ludwig, A.-K.; Romero, A.; Michalak, M.; Sherman, S. E.; Zhou, X.; Dazen, C.; Vertésy, S.; Kaltner, H.; Klein, M. L.; Gabius, H.-J.; Percec, V. Reaction of a Programmable Glycan Presentation of Glycodendrimersomes and Cells with Engineered Human Lectins to Show the Sugar Functionality of the Cell Surface. *Angew. Chem. Int. Ed.* **2017**, *56*, 14677–14681. (d) Xiao, Q.; Ludwig, A.-K.; Romano, C.; Buzzacchera, I.; Sherman, S. E.; Vetro, M.; Vertésy, S.; Kaltner, H.; Reed, E. H.; Möller, M.; Wilson, C. J.; Hammer, D. A.; Oscarson, S.; Klein, M. L.; Gabius, H.-J.; Percec, V. Exploring Functional Pairing Between Surface Glycoconjugates and Human Galectins Using Programmable Glycodendrimersomes. *Proc. Natl. Acad. Sci. U.S.A.* **2018**, *115*, E2509-E2518. (e) Rodriguez-Emmenegger, C.; Xiao, Q.; Kostina, N. Y.; Sherman, S. E.; Rahimi, K.; Partridge, B. E.; Li, S.; Sahoo, D.; Reveron Perez, A. M.; Buzzacchera, I.; Han, H.; Kerzner, M.; Malhotra, I.; Möller, M.; Wilson, C. J.; Good, M. C.; Goulian, M.; Baumgart, T.; Klein, M. L.; Percec, V. Encoding Biological Recognition in a Bicomponent Cell-Membrane Mimic. *Proc. Natl. Acad. Sci. U.S.A.* **2019**, *116*, 5376-5382.

(26) Peterca, M.; Percec, V.; Imam, M. R.; Leowanawat, P.; Morimitsu, K.; Heiney, P. A. Molecular Structure of Helical Supramolecular Dendrimers. *J. Am. Chem. Soc.* **2008**, *130*, 14840–14852.

(27) Wu, Y.-C.; Leowanawat, P.; Sun, H.-J.; Partridge, B. E.; Peterca, M.; Graf, R.; Spiess, H. W.; Zeng, X.; Ungar, G.; Hsu, C.-S.; Heiney, P. A.; Percec, V. Complex Columnar Hexagonal Polymorphism in Supramolecular Assemblies of a Semifluorinated Electron-Accepting Naphthalene Bisimide. *J. Am. Chem. Soc.* **2015**, *137*, 807–819.

(28) Heiney, P. A. Datasqueeze: A Software Tool for Powder and Small-Angle X-Ray Diffraction Analysis. *Comm. Powder Diffr. Newsl.* **2005**, *32*, 9–11.

(29) Klug, A.; Crick, F. H. C.; Wyckoff, H. W. Diffraction by Helical Structures. *Acta Cryst.* **1958**, *11*, 199–213.

(30) Lei, T.; Wang, J.-Y.; Pei, J. Roles of Flexible Chains in Organic Semiconducting Materials. *Chem. Mater.* **2014**, *26*, 594–603.

(31) (a) Janiak, C. A Critical Account on π–π Stacking in Metal Complexes with Aromatic Nitrogen-Containing Ligands. *J. Chem. Soc. Dalt. Trans.* **2000**, 3885–3896. (b) Sygula, A.; Fronczek, F. R.; Sygula, R.; Rabideau, P. W.; Olmstead, M. M. A Double Concave Hydrocarbon Buckycatcher. *J. Am. Chem. Soc.* **2007**, *129*, 3842–3843.

(32) Partridge, B. E.; Leowanawat, P.; Aqad, E.; Imam, M. R.; Sun, H.-J.; Peterca, M.; Heiney, P. A.; Graf, R.; Spiess, H. W.; Zeng, X.; Ungar, G.; Percec, V. Increasing 3D Supramolecular Order by Decreasing Molecular Order. A Comparative Study of Helical Assemblies of Dendronized Nonchlorinated and Tetrachlorinated Perylene Bisimides. *J. Am. Chem. Soc.* **2015**, *137*, 5210–5224.

(33) Suraru, S.-L.; Würthner, F. Strategies for the Synthesis of Functional Naphthalene Diimides. *Angew. Chem. Int. Ed.* 2014, 7428–7448.

(34) (a) Feng, X.; Wu, J.; Ai, M.; Pisula, W.; Zhi, L.; Rave, J. P.; Müllen, K. Triangle-Shaped Polycyclic Aromatic Hydrocarbons. *Angew. Chem. Int. Ed.* **2007**, *46*, 3033–3036. (b) Dong, R.; Pfeffermann, M.; Skidin, D.; Wang, F.; Fu, Y.; Narita, A.; Tommasini, M.; Moresco, F.; Cuniberti, G.; Berger, R.; Müllen, K.; Feng, X. Persulfurated Coronene: A New Generation of "Sulflower". *J. Am. Chem. Soc.* **2017**, *139*, 2168–2171.

(35) Percec, V.; Won, B. C.; Peterca, M.; Heiney, P. A. Expanding the Structural Diversity of Self-

Assembling Dendrons and Supramolecular Dendrimers *via* Complex Building Blocks. *J. Am. Chem. Soc.* **2007**, *127*, 11265–11278.

(36) Su, Z.; Zhang, R.; Yan, X.-Y.; Guo, Q.-Y.; Huang, J.; Shan, W.; Liu, W.; Liu, T.; Huang, M.; Cheng, S. Z. D. The Role of Architectural Engineering in Macromolecular Self-Assemblies *via* Non-Covalent Interactions: A Molecular LEGO Approach. *Prog. Polym. Sci.* **2020**, *103*, 101230.

(37) (a) Balagurusamy, V. S. K.; Ungar, G.; Percec, V.; Johansson, G. Rational Design of the First Spherical Supramolecular Dendrimers Self-Organized in a Novel Thermotropic Cubic Liquid-Crystalline Phase and the Determination of Their Shape by X-ray Analysis. *J. Am. Chem. Soc.* **1997**, *119*, 1539–1555. (b) Hudson, S. D.; Jung, H.-T.; Percec, V.; Cho, W.-D.; Johansson, G.; Ungar, G.; Balagurusamy, V. S. K. Direct Visualization of Individual Cylindrical and Spherical Supramolecular Dendrimers. *Science* **1997**, *278*, 449–452. (c) Percec, V.; Ahn, C.-H.; Ungar, G.; Yeardley, D. J. P.; Möller, M.; Sheiko, S. S. Controlling Polymer Shape through the Self-Assembly of Dendritic Side-Groups. *Nature* **1998**, *391*, 161–164. (d) Ungar, G.; Liu, Y.; Zeng, X.; Percec, V.; Cho, W.-D. Giant Supramolecular Liquid Crystal Lattice. *Science* **2003**, *299*, 1208–1211. (e) Zeng, X.; Ungar, G.; Liu, Y.; Percec, V.; Dulcey, A. E.; Hobbs, J. K. Supramolecular Dendritic Liquid Quasicrystals. *Nature* **2004**, *428*, 157–160. (f) Kim, K.; Schulze, M. W.; Arora, A.; Lewis III, R. M.; Hillmyer, M. A.; Dorfman, K. D.; Bates, F. S. Thermal Processing of Diblock Copolymer Melts Mimics Metallurgy. *Science* **2017**, *356*, 520–523. (g) Kim, S. A.; Jeong, K.-J.; Yethiraj, A.; Mahanthappa, M. K. Low-Symmetry Sphere Packings of Simple Surfactant Micelles Induced by Ionic Sphericity. *Proc. Natl. Acad. Sci.* **2017**, *114*, 4072–4077. (h) Huang, M.; Yue, K.; Wang, J.; Hsu, C. H.; Wang, L.; Cheng, S. Z. D. Frank-Kasper and Related Quasicrystal Spherical Phases in Macromolecules. *Sci. China Chem.* **2017**, *61*, 33–45. (i) Feng, X.; Zhang, R.; Li, Y.; Hong, Y.-L.; Guo, D.; Lang, K.; Wu, K.-Y.; Huang, M.; Mao, J.; Wesdemiotis, C.; Nishiyama, Y.; Zhang, W.; Zhang, W.; Miyoshi, T.; Li, T.; Cheng, S. Z. D. Hierarchical Self-Organization of AB_n Dendron-like Molecules into a Supramolecular Lattice Sequence. *ACS Ceent. Sci.* **2017**, *3*, 860–867. (j) Kim, K.; Arora, A.; Lewis, R. M.; Liu, M.; Li, W.; Shi, A.-C.; Dorfman, K. D.; Bates, F. S. Origins of Low Symmetry Phases in Asymmetric Diblock Copolymer Melts. *Proc. Natl. Acad. Sci.* **2018**, *115*, 847–854. (jk) Baez-Cotto, C. M.; Mahanthappa, M. K. Micellar Mimicry of Intermetallic C14 and C15 Laves Phases by Aqueous Lyotropic Self-Assembly. *ACS Nano* **2018**, *12*, 3226–3234. (l) Su, Z.; Hsu, C.; Gong, Z.; Feng, X.; Huang, J.; Zhang, R.; Wang, Y.; Mao, J.; Wesdemiotis, C.; Li, T.; Seifert, S.; Zhang, W.; Aida, T.; Huang, M.; Cheng, S. Z. D. Identification of a Frank-Kasper Z phase from Shape Amphiphile Self-Assembly. *Nat. Chem.* **2019**, *11*, 899–905. (m) Girard, M.; Wang, S.; Du, J. S.; Das, A.; Huang, Z.; Dravid, V. P.; Lee, B.; Mirkin, C. A.; Olvera de la Cruz, M. Particle Analogs of Electrons in Colloidal Crystals. *Science* **2019**, *364*, 1174–1178. (n) Lindsay, A. P.; Lewis, R. M.; Lee, B.; Peterson, A. J.; Lodge, T. P.; Bates, F. S. A15, σ, and a Quasicrystal: Access to Complex Particle Packings *via* Bidisperse Diblock Copolymer Blends. *ACS Macro Lett.* **2020**, 197–203.

(38) (a) Percec, V.; Wilson, D. A.; Leowanawat, P.; Wilson, C. J.; Hughes, A. D.; Kaucher, M. S.; Hammer, D. A.; Levine, D. H.; Kim, A. J.; Bates, F. S.; Davis, K. P.; Lodge, T. P.; Klein, M. L.; DeVane, R. H.; Aqad, E.; Rosen, B. M.; Argintaru, A. O.; Sienkowska, M. J.; Rissanen, K.; Nummelin, S.; Ropponen, J. Self-Assembly of Janus Dendrimers into Uniform Dendrimersomes and Other Complex Architectures. *Science* **2010**, *328*, 1009–1014. (b) Percec, V.; Leowanawat, P.; Sun, H.-J.; Kulikov, O.; Nusbaum, C. D.; Tran, T. M.; Bertin, A.; Wilson, D. A.; Peterca, M.; Zhang, S.; Kamat, N. P.; Vargo, K.; Moock, D.; Johnston, E. D.; Hammer, D. A.; Pochan, D. J.; Chen, Y.; Chabre, Y. M.; Shiao, T. C.; Bergeron-Brlek, M.; André, S.; Roy, R.; Gabius, H.-J.; Heiney, P. A. Modular Synthesis of Amphiphilic Janus Glycodendrimers and their Self-Assembly

into Glycodendrimersomes and Other Complex Architectures with Bioactivity to Biomedically Relevant Lectins. *J. Am. Chem. Soc.* **2013**, *135*, 9055–9077. (c) Sherman, S. E.; Xiao, Q.; Percec, V. Mimicking Complex Biological Membranes and Their Programmable Glycan Ligands with Dendrimersomes and Glycodendrimersomes. *Chem. Rev.* **2017**, *117*, 6538–6631. (d) Yadavalli, S. S.; Xiao, Q.; Sherman, S. E.; Hasley, W. D.; Klein, M. L.; Goulian, M.; Percec, V. Bioactive Cell-like Hybrids from Dendrimersomes with a Human Cell Membrane and Its Components. *Proc. Natl. Acad. Sci. U. S. A.* **2019**, *116*, 744–752. (e) Torre, P.; Xiao, Q.; Buzzacchera, I.; Sherman, S. E.; Rahimi, K.; Kostina, N. Y.; Rodriguez-Emmenegger, C.; Möller, M.; Wilson, C. J.; Klein, M. L.; Good, M. C.; Percec, V. Encapsulation of Hydrophobic Components in Dendrimersomes and Decoration of Their Surface with Proteins and Nucleic Acids. *Proc. Natl. Acad. Sci. U.S.A.* **2019**, *116*, 15378–15385. (f) Kostina, N. Yu.; Rahimi, K.; Xiao, Q.; Haraszti, T.; Dedisch, S.; Spatz, J. P.; Schwaneberg, U.; Klein, M. L.; Percec, V.; Möller, M.; Rodriguez-Emmenegger, C. Membrane-Mimetic Dendrimersomes Engulf Living Bacteria *via* Endocytosis. *Nano Lett.* **2019**, *19*, 5732–5738.

TOC Graphic

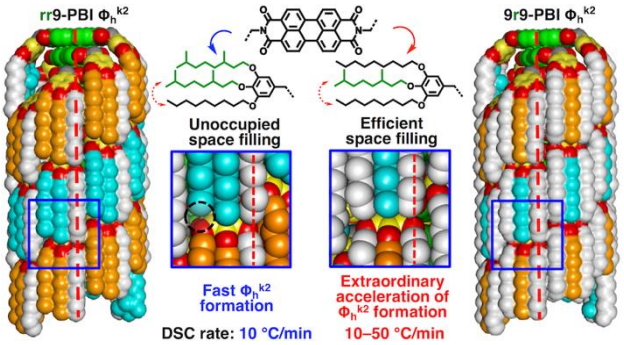
rr9-PBI Φh k2
9r9-PBI Φh k2
Unoccupied space filling
Efficient space filling
Fast Φh k2 formation
Extraordinary acceleration of Φh k2 formation
DSC rate: 10 °C/min
10–50 °C/min